Accepted Manuscript

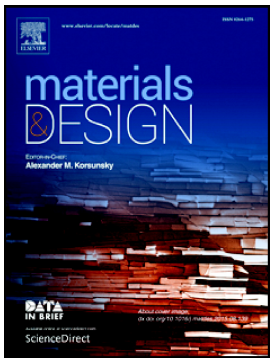

Impact of residual stress on thermal damage accumulation, and Young's modulus of fiber-reinforced ultra-high temperature ceramics

P. Galizia, L. Zoli, D. Sciti

PII: S0264-1275(18)30774-3
DOI: doi:10.1016/j.matdes.2018.10.019
Reference: JMADE 7433

To appear in: *Materials & Design*

Received date: 3 July 2018
Revised date: 4 October 2018
Accepted date: 12 October 2018

Please cite this article as: P. Galizia, L. Zoli, D. Sciti , Impact of residual stress on thermal damage accumulation, and Young's modulus of fiber-reinforced ultra-high temperature ceramics. Jmade (2018), doi:10.1016/j.matdes.2018.10.019

Impact of residual stress on thermal damage accumulation, and Young's modulus of fiber-reinforced ultra-high temperature ceramics

P. Galizia*, L. Zoli, D. Sciti

CNR-ISTEC, National Research Council of Italy - Institute of Science and Technology for Ceramics, Via Granarolo 64, I-48018 Faenza, Italy

*corresponding author, email: pietro.galizia@istec.cnr.it

Abstract

Ultra-high temperature ceramic matrix composites (*UHTCMCs*) based on ZrB_2-matrix reinforced with 45 vol% of unidirectional continuous carbon fibers are studied through the thermal mechanical hysteresis in order to investigate the thermal damage accumulation. The presented analysis allowed to extrapolate the Young's modulus of the matrix from thermal expansion measures. It is found out that the initial matrix Young's modulus of 195 GPa steadily decreases by thermal cycling the samples between RT and 1,300 °C as a consequence of matrix cracking. On the other hand, the analysis suggests that carbon fibers keep constant their Young's modulus at 780 GPa. Finally, the residual stresses due to the different coefficient of thermal expansion between matrix and carbon fibers are discussed and let to justify the Young's modulus of 230 GPa which cannot be explained with the so-called "rule of mixtures" generally valid and widely used in the composite science.

Keywords: boride; ceramic-matrix composite (CMC); pitch-derived carbon fiber; thermal expansion coefficient; thermomechanical hysteresis loops; linear elasticity.

1. Introduction

The demand for more powerful spacecraft engines and aircrafts with lower emissions is stimulating more research effort to raise the temperature capability of materials well over 1,500 °C [1]. In the last decade, the increasing severity of operating conditions of the future hypersonic vehicles [2-4] led to the development of

a novel class of ceramic matrix composites (*CMCs*) based on fiber-reinforced ultra-high temperature ceramics (*UHTCs*). Levine *et al.* in 2002 [5] fabricated a SiC fiber-reinforced ZrB_2 plus 20 vol.% SiC composite. However, due to the low fracture toughness, poor resistance to thermal shock, and low resistance to the aggressive oxidation, the authors claimed that the investigated composites were "not ready to be considered as aeropropulsion materials for any applications longer than a few minutes" [5]. The following efforts, on one hand, aimed at enhancing the thermomechanical properties/ablation resistance of C/C and C/SiC composites, by adding a certain amount of *UHTC* compounds through powder infiltration (*PI*) [6], chemical vapour infiltration (*CVI*) [7], polymer impregnation pyrolysis (*PIP*) [8], soft-solution [9], slurry infiltration [10], and reactive meting infiltration (*RMI*) [11,12]. On the other hand, continuous fiber-reinforced *UHTCs* produced, since 2004, by *CVI* [13], *RMI* [14], precursor infiltration and pyrolysis process [15] were characterized by wound ceramic matrix, which may strongly affect the material performances. The combination of high flaw tolerance of CMC [16], with the high erosion/oxidation resistance and thermal stability of *UHTCs* (e.g. refractory borides and carbides of early transition metals) [17-20], was achieved by Zoli and Sciti [21] in 2017. They rapidly developed a baseline *UHTCMC* mainly based on ZrB_2 matrix reinforced with around 45 vol.% of C_f [22-25]. The flexural strength at RT and 1,500 °C, and the fracture toughness were increased up to 360 MPa, 550 MPa, and 11 $MPa \cdot m^{1/2}$, respectively [25,26]. These results, together with the obtained critical flaw size (230-470 µm at RT [25,26], 80 µm at 1,500 °C [25]), the retained strength of 310 MPa after water-quenching, from 1,500 °C to 20 °C of bath temperature [25], the good oxidation behaviour up to 1,500 °C [19], and the absence of appreciable ablation under high velocity oxy-fuel torch (*HVOF*) [2,27,28], confirm the potential of *UHTCMCs* as candidates for reusable thermal protection systems (*TPSs*) for commercial space travel and exploration. In spite of the progress done, *UHTCMCs* still show a considerable margin for further development. In particular, the developed baseline materials may be affected by the coefficient of thermal expansion (*CTE*) mismatch between the matrix and the fiber [20,29]. It was observed that the high *CTE* difference between ZrB_2 and C_f induces flaws formation during cooling from the sintering temperatures, and leaves a high residual stress level that has an impact on the final composite properties [25].

In this work, we investigate the thermomechanical behaviour of unidirectional C_f-reinforced ZrB_2-matrix (the above mentioned "baseline *UHTCMC*") [25] through a simple thermal dilatometry analysis. In spite of

its simplicity, our analysis allows to (*i*) characterize the thermal dilatation of the unidirectional UHTCMC along the longitudinal and transverse directions, (*ii*) calculate the anisotropy degree of the composite, and (*iii*) calculate the Young's modulus of the matrix. (*iv*) By thermal cycling the samples, we present a *modus operandi* to characterize the thermal damage accumulation and the thermomechanical stability (a key parameter for the designing of reusable components subjected to thermal cycles). In fact, we show how the evolution of *CTE* response as function of thermal cycles, and the hysteresis loops are correlated to the damage accumulation, and can be used to calculate the Young's modulus variation of the matrix. Finally, by taking into account the residual stresses, a novel model for the linear elastic zone is presented and discussed. This model is meant to replace the first zone of the *ACK* model [30] where the slope of the stress-strain curve should follow the rule of mixtures of the main constituents. This last achievement can bring enormous benefits to the advanced modeling and design of *CMC*-components mechanical behaviour, which is still an open issue [31,32]. In particular, the proposed model (*i*) allows a better prediction and understanding of the elastic properties and progressive damage of different composite materials, and (*ii*) will push forward the application of *CMC*-components in the fields of aerospace and civil engineering.

2. Material and methods

UHTCMCs based on carbon fiber-reinforced ZrB_2 were produced by hot pressing at 1900 °C. The final microstructure consists in 55 vol. % of matrix (83 % ZrB_2 + 10 % SiC + 7 % pores), and 45 vol. % of homogeneously distributed unidirectional carbon fiber, C_f (so forth called *UD*). Further details on slurry preparation, infiltration, densification, and microstructural and mechanical features of the produced samples are reported in previously published work [25].

The microstructure was analyzed on polished and fractured surfaces by field emission scanning electron microscopy (FE-SEM, Carl Zeiss Sigma NTS Gmbh Öberkochen, Germany).

The relative dimensional change ($\Delta L/L_0$) versus temperature was measured up to 1,300 °C under flowing argon with a 5 °C/min heating rate using a dilatometer Netzsch mod. DIL E 402 (Netzsch, Geraetebau, Germany), on 25 mm x 2.5 mm x 2 mm bars. $\Delta L/L_0$ of *UD* was measured along transverse and longitudinal orientation of the C_f. The thermal cycling up to 1300 °C was carried out on the longitudinal direction of C_f, where the thermal dilatations mismatch between matrix and fiber is maximized.

3. Results and discussion

3.1 Microstructural features

The typical microstructure of the baseline composite (*UD*) is shown in Fig.1. The fibers are all aligned in the same direction in order to create an simplified texture for analysis and interpretation of the mechanical behaviour. The transverse cross section (Fig.1 (a)) displays a homogeneous fiber distribution in the dense matrix and the jagged fiber/matrix interfaces. The longitudinal cross sections show the anisotropic microstructure of the carbon fibers (Fig.1 (b)), the presence of voids between the graphitic layers (Fig.1 (b)), the interlocked fiber/matrix interfaces (Fig.1 (b)), and the cracks in the matrix (Fig.1 (c)) that are homogenelusly spaced with a periodicity of 20 – 40 micron.

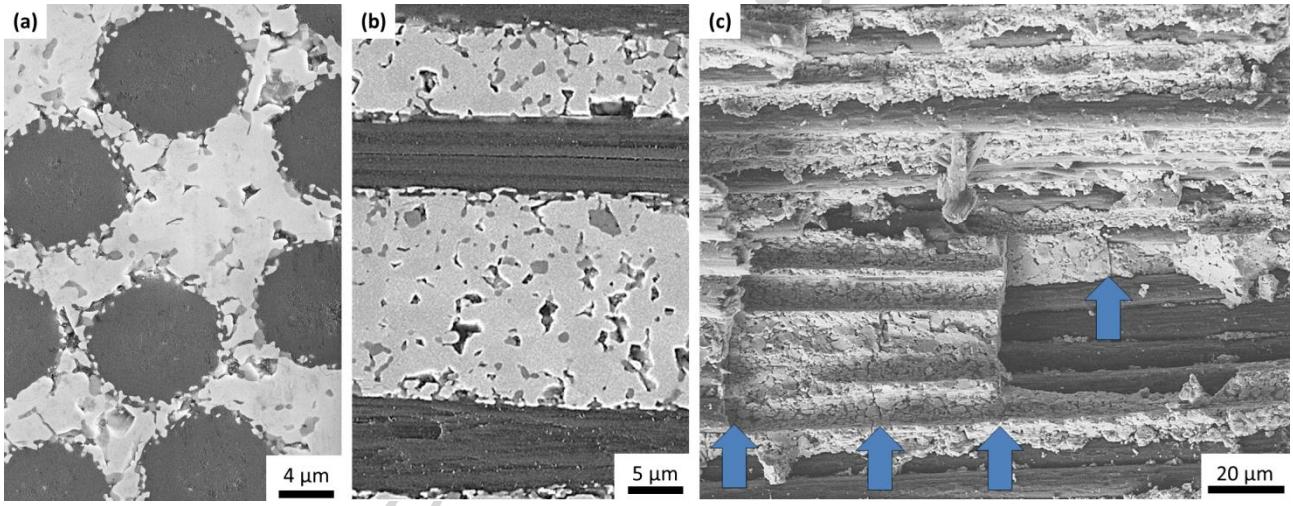

Fig.1. SEM micrographs of polished cross section of *UHTCMC* based on pitch-derived carbon fibers and ZrB_2/SiC matrix along (a) the transverse direction, and (b) longitudinal direction. (c) Fracture surface along the longitudinal direction (the arrows point the presence of cracks in the matrix). *(two- column)*

3.2 Thermomechanical analysis: a powerful method to determine CTE, coefficient of anisotropy, matrix modulus

Experimental curves in Fig.2 (a) show the relative dimensional change ($\Delta L/L_0$) versus temperature up to 1,500 °C for polycrystalline ZrB_2 [20], typical anisotropic pitch-derived carbon fibers (C_f) [29], and unidirectional C_f-reinforced ZrB_2-matrix of this work (*UD* samples), in both directions: along the transverse (*t* subscript) and longitudinal direction (*l* subscript). It can be seen that for C_f, $\Delta L/L_0$ along the transverse

section is strongly dependent on the temperature, but nearly constant in the longitudinal direction. Also, we can observe that the elongations ($\Delta L/L_0$) in the transverse direction of the *UD* composite and of C_f are very close to each other and also very comparable with that of a bulk isotropic ZrB_2. This is consistent with the microstructural observation that few or no microcracks were generally found in the ZrB_2 matrix in the transverse cross section of the composite. Looking more carefully, we can see that C_f displays a slightly higher value within the entire investigated temperature range than the isotropic ZrB_2 material.

The higher *CTE* of C_f and the presence of the weak van der Waals interactions between the carbon layers within the fibers could be the reason of the intensification of voids observed in the C_f sections after densification, with respect to those occasionally present in the as-produced fibers [33]. During cooling, void formation compensates the higher transverse thermal shrinkage of C_f. In fact, since C_f are physically well-joined with the ZrB_2 matrix – it was found out that matrix shrinkage during the densification process produces strongly jagged ZrB_2/C_f [26] – the biaxial tension (along the transverse directions) and uniaxial compression (along the longitudinal direction), seems to favour the carbon layers sliding among themselves rather than delamination at the ZrB_2/C_f interface. This mechanical interlocking developed at the ZrB_2/C_f interfaces transfers the C_f anisotropy to the *UD* samples: for this reason $(\Delta L/L_0)_{UD,l}$ is much lower and much less dependent on the temperature compared to $(\Delta L/L_0)_{UD,t}$ (Fig.2 (a)). This aspect should be taken into account especially when *UHCMCs* are designed with more complex structure with respect to the unidirectional configuration, *e.g.* 0° / 90° cross-ply configuration.

Let's us now evaluate the degree of anisotropy as function of temperature, *R(T)* of *UD* composite and C_f. For the composite and the fiber, *R* is calculated using the experimental values of transverse (*t*) and the longitudinal (*l*) relative dimensional change ($\Delta L/L_0$) [29]:

$$R(T) = \frac{\left(1+\left(\frac{\Delta L}{L_0}\right)_t\right)}{\left(1+\left(\frac{\Delta L}{L_0}\right)_l\right)} - 1 \quad (1)$$

For instance, in the case of isotropic bulk ZrB_2 *R(T)* = 0. The values obtained from Eq.1 are plotted in Fig.2 (b). On the other hand, for the sake of comparison, we calculated the theoretical value of *R(T)* for the *UD* composite with the micromechanical model, making the following assumptions:

- the two components are perfectly bonded together forming a simple beam so that they deform together (*i.e.* iso-strain condition);

- no external load is applied so that the overall stresses in the longitudinal direction of the beam are balanced (*i.e.* equilibrium condition);

- along the transverse direction there is no *CTE* difference between the matrix and the transversely isotropic fibers [33]. Hence the composites *CTE* is the same as the side phases.

In the above conditions, the theoretical $(\Delta L/L_0)_{l,c}$ of the *UD* sample is modeled by the Schapery's model [34]:

$$\left(\frac{\Delta L}{L_0}\right)_{l,c} = \frac{\left(\frac{\Delta L}{L_0}\right)_{l,f} E_f V_f + \left(\frac{\Delta L}{L_0}\right)_m E_m(1-V_f)}{E_f V_f + E_m(1-V_f)} \quad (2)$$

where the subscripts '*m*', '*f*', and 'c' refer to matrix, fiber, and composite, respectively, *V* is the volume fraction, and *E* is the Young's modulus. In our case, the theoretical $(\Delta L/L_0)_{l,c}$ of the *UD* sample is calculated by fixing V_f = 0.45, E_f = 780 GPa, and E_m = 420 GPa [20], and imposing thermal dilatation of the side phases: C_f [29], and ZrB_2 [20]. Hence, the theoretical *R(T)* is obtained by using in the denominator of Eq.1 the theoretical $(\Delta L/L_0)_{l,c}$ instead of the experimental value ($(\Delta L/L_0)_{UD,l}$ curve plotted in Fig.2 (a)). It is worthy to note that, along the transverse direction, there is not significant difference between the theoretical $(\Delta L/L_0)_{t,c}$ and the experimental one, since $(\Delta L/L_0)_{Cf,t}$ and $(\Delta L/L_0)_{ZrB2,t}$ are quite similar to $(\Delta L/L_0)_{UD,t}$. Looking at the curves in Fig.2 (b), we can see that the anisotropy, *R(T)*, increases with increasing the temperature for C_f as well as for *UD* samples. At 1,500 °C the anisotropic degree value for C_f is 1.03, whilst in the *UD* composite *R* is reduced to 0.71 owing to the isotropic behaviour of the matrix (*R* = 0). However, the obtained value of *R(*1500°C*)* = 0.71 is much higher than the expected one: *R(*1500°C*)* = 0.39. The key to understand the reasons for this discrepancy is in the longitudinal $\Delta L/L_0$contribution of the *UD* sample, that should be much higher.

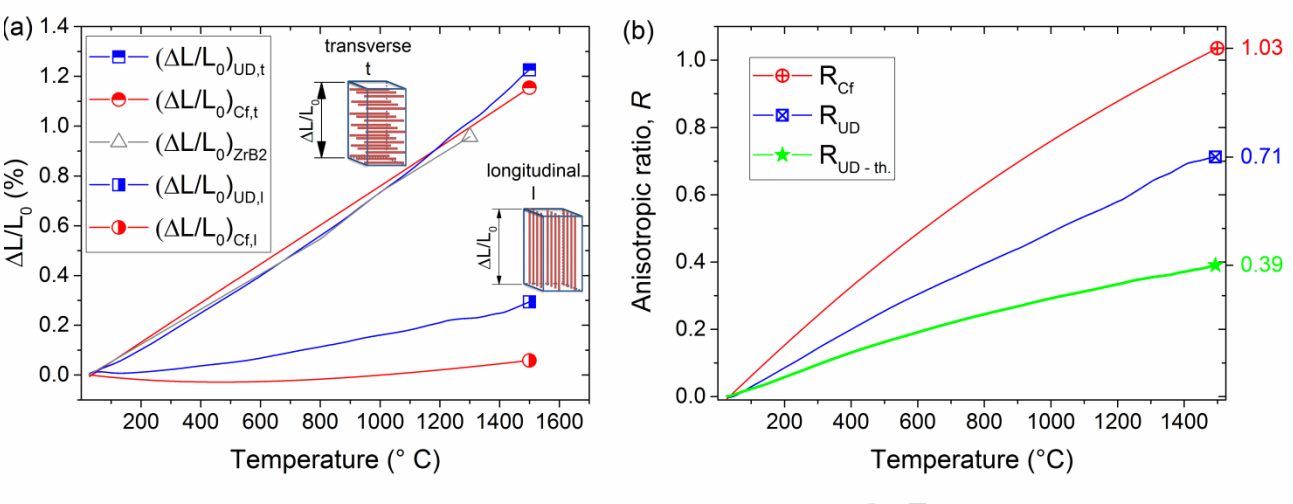

Fig.2. (a) Relative dimensional change ($\Delta L/L_0$) vs. temperature of the tested *UD* samples (blue line with square symbols), and pitch-derived fibers C_f [29] (red line with circle symbols) along the transverse (*t* subscript, half up symbols) and the longitudinal (*l* subscript, half right symbols) direction, and polycrystalline ZrB_2 [20] (gray line with open triangle symbol). (b) Anisotropy degree *R* vs. temperature of tested *UD* (blue line with marked square symbol), C_f (red line with marked circle symbol), and theoretical *UD* trend (green line with solid star symbol). *(two- column)*

In fact, as it can be seen in Fig.3, the theoretical $(\Delta L/L_0)_l$, calculated trough the Eq.2, is higher than the experimental one. This is usually due to mechanical discontinuities in the materials such as pores and/or cracks. Since the voids inside C_f do not affect the mechanical behaviour in the longitudinal direction, we believe that a major role is played by matrix cracking [33]. Cracks have a strong detrimental effect on the E_m value owing to their high surface/volume ratio. This detrimental effect is commonly modelled by the following exponential relationship [35]:

$$E = E_{th}e^{-bp} \quad (3)$$

where E, and E_{th} are the Young's modulus of the real material and the fully dense one, respectively, p is the voids volumetric fraction, and b is a numerical constant that takes into account the shape and stacking of the voids. The value of the latter is attested in the range of about 2 - 4 in case of sintering porosity, and can be higher than 9 in the stricter conditions as in the presence of multiple interacting cracks [36]. Thus, considering b = 9 – 13, p = 5 – 10 vol%, and E_{th} = 420 GPa, the Young's modulus of the matrix could be attested between 114 GPa and 268 GPa. A measure of E_m can be extrapolated by fitting the experimental

values ($(\Delta L/L_0)_{UD,l}$) with Eq.2. By releasing only the E_m value into the theoretical $(\Delta L/L_0)_{l,c}$ (Eq.2), the fitting convergence is reached by decreasing E_m from 420 GPa down to 195 GPa (Fig.3). Similarly, the matrix cracking causes the much lower flexural strength, σ = 65 MPa [25], of the matrix with respect to the corresponding bulk material σ = 600 MPa [20]. All the above considerations suggest that mechanical and thermomechanical behaviours of the *UD* samples are mainly controlled by C_f simply because the matrix is strongly damaged.

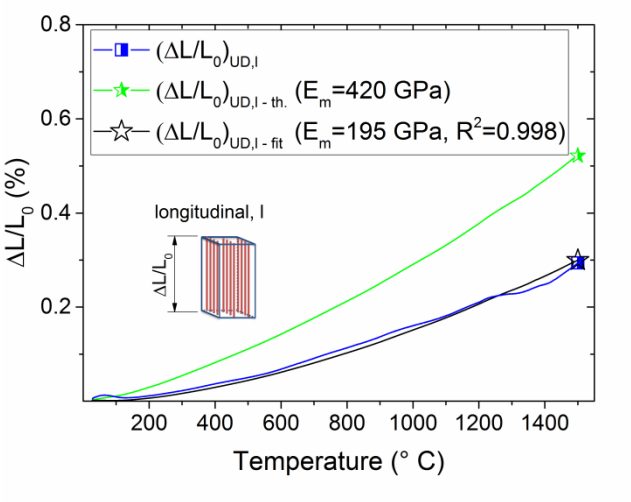

Fig.3. Relative dimensional change ($\Delta L/L_0$) along *l*-direction vs. temperature of the tested *UD* samples (blue line with square symbols), theoretical trend (green line with half right star symbols), and adjusted trend which take into account the matrix damaging/softening (black line with open star symbols). *(single column)*

3.3 Residual stress build up and matrix cracking

Cracks in the matrix are generated by residual stresses developed during cooling in case that neither the matrix nor the fibers exhibit time-dependent deformation (*i.e.* creep). In fact, during cooling under the 'joining' temperature of about 1,550 °C [36] the internal stresses, σ_0, should follow the trends plotted in Fig.4 (b), which were calculated with the following equations:

$$\sigma_{0,f} = \left[\left(\frac{\Delta L}{L_0}\right)_{l,f} - \left(\frac{\Delta L}{L_0}\right)_{l,c}\right] E_f \quad (4)$$

$$\sigma_{0,m} = \left[\left(\frac{\Delta L}{L_0}\right)_{m} - \left(\frac{\Delta L}{L_0}\right)_{l,c}\right] E_m \quad (5)$$

In the above equations the Young's moduli are considered temperature dependent in order to account for the material softening with the temperature. In particular E_m is set to follow the empirical Watchman's equation [37,38]:

$$E_m(T) = E_m - bT\, e^{\frac{-T_0}{T}} \quad (6)$$

where the constants b and T_0 are fixed to 0.0399 and 193 K [38]. The magnitude of the calculated stresses is lower than the tensile strength of the fibers (which is over 4 GPa), but is not small enough to avoid the local failure of the matrix. According to Eq. 5 a thermal difference of 365 °C is enough to overcome the tensile strength of the ZrB_2 and should lead to cracks formation in order to allow the matrix shrinkage which is accompanied by stress release. Unfortunately, it is not easy to quantify the residual stress in the matrix, and to understand the effect of the high level of compressional stress into the fibers. All the performed microstructure analyses on the produced *UHTCMCs* shown no evidence of macroscopic fiber kink or buckling. This lack of evidence is reasonable due to the high stiffness of the matrix, but, inside the fibers, kink and buckling phenomena could occur at the scale of the alignment of graphene sheets along the fiber axis. The SEM analysis confirms the presence of the pores (Fig.1 (b)) and cracks (Fig.1 (c)) due to the biaxial and uniaxial tension, respectively, developed during cooling. In particular, it is worthy to note how the biaxial tension not only produces pores inside C_f, but, in some case, where C_f are not well distributed, we observe a strong deformation of C_f shape (not shown here). On the other side, along the longitudinal direction, it is not surprising that the high *CTE* difference leads to a small crack spacing which is attested at about 20-40 µm (Fig.1 (c)). The evidence of the transverse cracks is in accordance with the above calculated build up in residual stress (1.6 MPa/°C of average value of the residual longitudinal stress) and with the fact that the load between matrix and fibers is transmitted by shear stresses which cannot rise above the matrix shear strength.

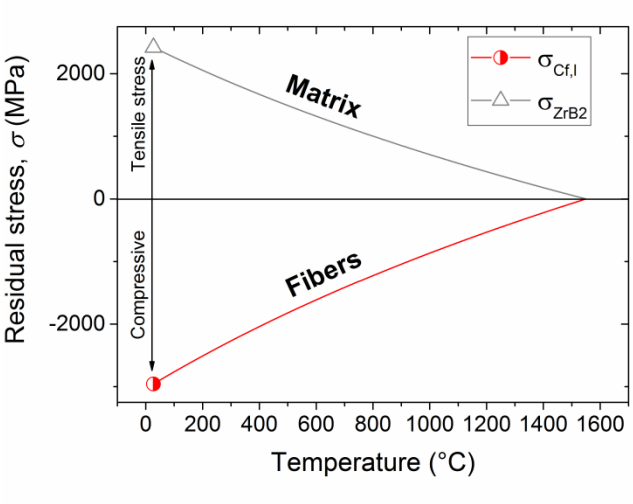

Fig.4. Theoretical residual stresses into matrix (gray line with open triangle symbol) and fibers (red line with half right circle symbols) that should develop during cooling. *(single column)*

3.4 Thermal cycling and damage accumulation

Owing to the high *CTE* difference between matrix and fibers, it is reasonable to suppose that the observed crack spacing of 20-40 µm (as point out by the arrows in Fig.1 (c)) is not that of equilibrium. In fact, by thermomechanical cycling the *UD* samples, hystereses were found (Fig.5 (a)), and should be mainly attributed to the crack formation. Moreover, the cracks formation at each thermal cycle leads to a residual permanent expansion which is the consequence of the compressional strains released by fibers and the discontinuity produced in the matrix. It can be seen that the initial dimension at *RT*, L_0, gradually increases up to 0.11%, 0.19 %, and 0.35% after the first, second, and third thermal cycle, respectively. By rescaling the measured ($\Delta L/L_0$) curves in agreement with these increments (Fig.5 (b)), it can be seen how the ($\Delta L/L_0$) curves gradually approach the $\left(\frac{\Delta L}{L_0}\right)_{l,f}$ trend. This suggests that the fibers keep their initial modulus, which, becoming increasingly bigger than matrix modulus, imposes their thermal expansion [39]. In particular, with the third rising (III-5 curve) at about 550 °C – 750 °C, *UD* sample expands as free C_f. This means that cracks formed during thermal cycles allow the free expansion and shrinkage of the matrix and fibers, respectively, up to 750 °C, roughly. The free matrix expansion is highlighted by the presence of the "bell" between *RT* and 100 °C, and the free fiber shrinkage is clearly visible by the ($\Delta L/L_0$) decreasing up to 600 °C. Above 600 °C the higher matrix *CTE* pushes up the ($\Delta L/L_0$) values of the *UD* sample with respect to that of C_f. In this way, stresses start to increase again and can produce further cracks formation as it is evidenced by the slope

increase above 1,200 °C, which produces the matrix expansion (detected by the thermomechanical analysis, *TMA*) and the fiber shrinkage (not detectable). The decline of the elastic properties of the matrix was quantified by fitting ($\Delta L/L_0$) curves with Eq. 2. The fitting (Fig.5 (b)) was performed only in the part of the ($\Delta L/L_0$) curves where matrix and fiber mechanically interact (*i.e.* mechanical constrained) without producing evident cracks formation. This reasonably occurs in the range between 650 °C and 1,000 °C. The fitting (Fig.5 (b)) shows a steady decrease of E_m which goes from the 195 GPa of the as sintered sample to 164 GPa with the first thermal cycle and then drops down to 59 GPa and 24 GPa with the following two cycles. This means that the high *CTE* difference severely afflicts the matrix which from one side releases its residual tensile stress, but on the other losses its mechanical continuity [40-42]. Anyway, the residual stress release by the cracks formation could be a minor concern, since these materials are intrinsic 'damage-tolerant' and 'notch-insensitive', show an increase of strength after thermal shock, and can be shocked at temperatures higher than 1,480 °C [25]. This behaviour has been correlated to cracks formation under the critical value per unit volume after thermal shock which has led to the residual stress release. Similar results were obtained with fatigue tests where the fully-developed micro-damaging led to more uniform stress state and a consecutive residual strength higher than the pristine ultimate strength [42,43]. On the other hand, the fiber compression state can be exploited for structural application at RT, since the enhanced crack bridging by the fiber – greater applied stress must be imposed on the fibers to attain their fracture stresses - enhances the toughening [44].

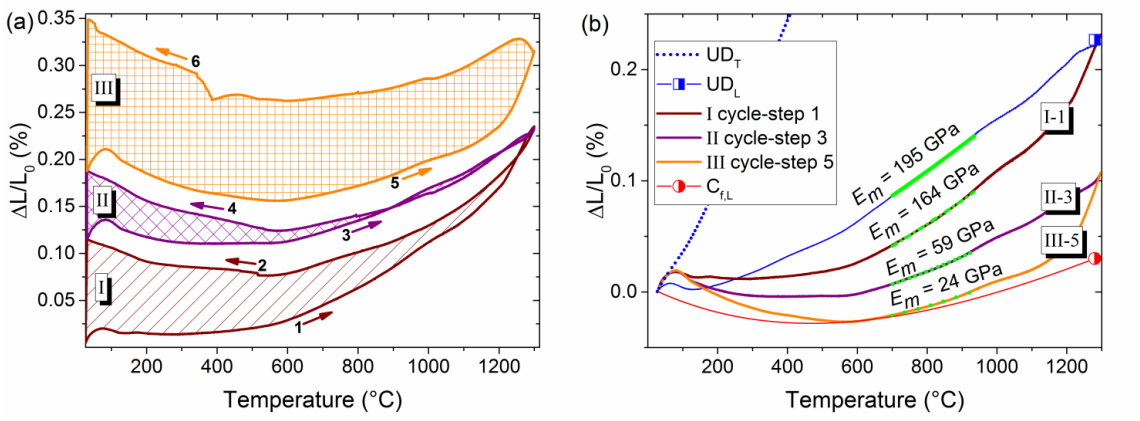

Fig.5. (a) Relative dimensional change ($\Delta L/L_0$) along *l*-direction during three consecutive thermal cycles (labeled with roman numbers) between *RT* and 1300 °C. Each thermal step is numbered in chronological order. (b) Relative dimensional change ($\Delta L/L_0$) along *l*-direction for each heating step together with the $\Delta L/L_0$ of typical anisotropic pitch-derived carbon fibers (C_f) [27], and that of *UD* samples after sintering (plotted also in Fig.2). The curves were scaled by updating the L_0 value after each thermal cycle. *(two- column)*

3.5 Composite Young's modulus and the "springs' theory"

The effect of residual stresses - caused by the matrix/fiber CTE mismatch when cooling to ambient temperature after densification – on mechanical strength at RT and high temperature, fatigue damage, fatigue life, and thermal shock was studied by several authors [25,41,42,45]. However, no explanation, to the best of our knowledge, is given about the effect of the residual stresses on the macroscopic elastic modulus prior to microdamage development. In ref. [45], Ziegler shows how the thermal stresses influence the flexural strength of SiC fiber-reinforced glass composites, but no attempts are made to explain the Young modulus decrease from about 125 GPa to 75 GPa with the increasing of the thermal stress from $2.09 \cdot 10^{-6}$ °C^{-1} to $6.6 \cdot 10^{-6}$ °C^{-1}. Reynaud et al. [46] show that tensile mean elastic modulus of SiC/SiC *CMC* reaches the value of the compressive mean elastic modulus when thermal residual stresses are released under fatigue test, but they did not provide a suitable explanation. Shi et al. [47] demonstrate how the residual stress influence the effective Young's modulus of cantilever beams. In our case, since the residual stresses should be close to the critical values, the Young's modulus should be strongly affected. In fact, in our previous work [25], we found out a longitudinal Young's modulus of 232±10 GPa which is completely in disagreement with the expected one calculated with the following Voigt's equation (the conventional rule of mixture):

$$E_c = E_f V_f + E_m(1 - V_f) \quad (7)$$

Whatever value from 420 down to 0 GPa is attributed to E_m, Eq. 6 gives a higher result with respect to the value experimentally measured. This simple observation demonstrates that the decrease in the Young modulus of *UHTCMCs* cannot be attributed just to matrix damage [48], but a direct contribution from residual stresses should be added even in absence of defects. In fact, since the fibers are compressed and the matrix is stretched, they would tend to expand and shrink, respectively. Hence, when an external tensile force is applied the matrix will counteract the applied tensile force as prescribed by Hooke's law, and the fibers (in the iso-strain condition: $\varepsilon_m = \varepsilon_f = \varepsilon$) will spontaneously follow the expansion releasing part of the bounded energy due to the initial thermal stress ($\sigma_{0,f}$) and strain ($\varepsilon_{0,f}$): $U_{0,f} = \frac{1}{2}\int_V (\sigma_{0,f}\varepsilon_{0,f})\, dV$. In the opposite case, under external compressional force, the compressed fibers will promptly respond to the mechanical stimulus by increasing their compressional strain according to their stiffness (E_f = 780 GPa since the anisotropic pith-derived fiber are just in an initial compressional state and are constrained with the hard matrix, the compressional modulus value can be considered equal to the tensile one) while the matrix will supply the bounded energy: $U_{0,m} = \frac{1}{2}\int_V (\sigma_{0,m}\varepsilon_{0,m})\, dV$. The above discussion can be visualized in the sketch of Fig.6.

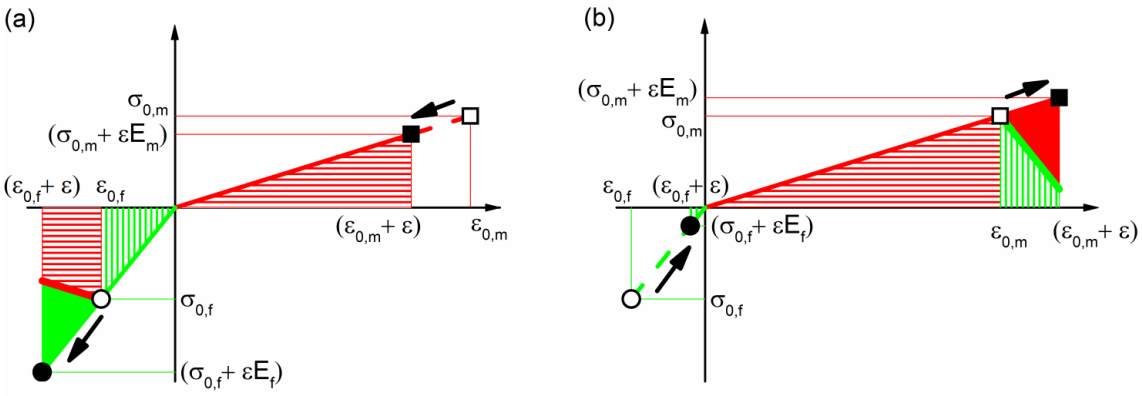

Fig.6. Scheme of the stress – strain variation after applying a compressive (a) and tensile (b) external load into a continuous fiber-reinforced composite with initial/residual thermal stresses. The arrows flow from the initial point (open symbols) to the final point (solid symbols) for both fiber (circle symbols) and matrix (square symbols). The areas filled with lines pattern (horizontal for matrix, vertical for fiber) correspond to the initial/bounded energy density. The solid areas correspond to deformation work done by the external applied force. *(two- column)*

According to the linear theory of elasticity, when an external force (F) is applied the variation in strain energy density ($W = U/dV$) is:

$$\Delta W = \left(\frac{1}{2}\left(\sigma_{0,f} + E_f\varepsilon\right)\left(\varepsilon_{0,f} + \varepsilon\right) + \frac{1}{2}\left(\sigma_{0,m} + E_m\varepsilon\right)\left(\varepsilon_{0,m} + \varepsilon\right)\right) - \left(W_{0,f} + W_{0,m}\right) \quad (8)$$

Since the residuals stresses ($\sigma_{0,m}$ and $\sigma_{0,f}$) are equilibrated in absence of external forces, and the directions of strain and stress are the same in one case and opposite in the other case, Eq.8 reduces to:

$$\Delta W = \frac{1}{2}\left|E_f - E_m\right|\varepsilon^2 \quad (9)$$

The variation in stress, due to the variation in strain imposed by the external force, is:

$$\frac{d\Delta W}{d\varepsilon} = d\sigma = \left|E_f - E_m\right|d\varepsilon \quad (10)$$

Hence, the equivalent longitudinal elastic modulus of a portion of unidirectional continuous fiber-reinforced composite, where matrix/fiber interface are not debonded and the entire matrix and fiber volumes are strained, is:

$$E_{eq} = \left|E_f V_f - E_m\left(1 - V_f\right)\right| \quad (11)$$

Assuming that close to the matrix/fiber interface matrix cracks and to the debonded area has no longer residual stress, the overall elastic modulus of the fiber can be described as a series of thermally strained and

unstrained fibers. Thus, the overall fiber elastic modulus can be modeled through the Reuss' approximation (the as called inverse rule of mixture):

$$E_{eq,f} = \frac{E_{eq}\,E_f}{E_f d + E_{eq}(1-d)} \tag{12}$$

where *d* is fraction of debonded fiber/matrix interface. Since the observed crack frequency is 0.05 - 0.1 μm^{-1}, the overall Young's modulus calculated trough the mixed rule between the Eq.(3) and (12) is 222 ±18 GPa, which matches the measured value.

It is evident that the high matrix/fiber *CTE* mismatch, the jagged matrix/fiber interface (which requires a change in the concept of pure shear load transfer [49,50]), and other strong chemo-physical differences between matrix and fiber, configure the *UHTCMCs* as a novel class of composites materials. Although this class of materials presents critical issues, it has also shown superior properties for the aerospace applications and more generally harsh environments. Hence, in our opinion it is important to dedicate much more effort in the study and development of *UHTCMCs* in order to exploit their potential as much as possible.

4. Conclusion

The present work has shown that (*i*) the strong jagged C_f/ZrB_2 interfaces transfer the anisotropic behaviour of C_f to the entire composite. (*ii*) The high *CTE* mismatch between ZrB_2 based matrix and pitch-derived carbon fiber along their longitudinal direction causes cracks formation during cooling from the sintering temperature. (*iii*) A general modus operandi based on the Schapery's model was suggested to estimate the Young's modulus of the single components, *i.e.* matrix and fiber. (*iv*) The as sintered matrix is characterized by a Young's modulus of 195 GPa, instead of 420 GPa shown by similar bulk ceramics, due to the cracks formation. (*v*) The longitudinal thermal dilatation decreases by thermal cycling and, due to the damage accumulation, gradually approaches the dilatation behaviour of bare carbon fibers. (*vi*) The experimental data in agreement with the Schapery's model suggest that carbon fibers are affected by neither sintering process nor thermal cycles in Ar atmosphere. (*vii*) Taking into account the damaging of the matrix and the residual stresses distribution, we proposed a modification - called the "springs' theory" - of the law of mixtures in order to explain the measured 230 GPa of Young's modulus for the *UD* composites along the longitudinal direction. These results are particularly important for the understanding of this novel class of materials and

paves the way for new developments of different composite materials. On one side, the proposed method to calculate the Young's modulus of the matrix is useful to easily check the matrix contribution to the overall composite behaviour and its stability to the thermal cycles. On the other side, the proposed model is of great value for the accurate prediction and assessment of the elastic and failure properties of *CMC*-components.

Acknowledgements

The research leading to these results has received funding from the European Union's Horizon 2020 Programme under grant agreement C3HARME No. 685594. The authors are grateful to E. Landi for thermal dilatometric measurements.

References

[1] N.P. Padture, Advanced structural ceramics in aerospace propulsion, Nat. Mater. 15 (2016) 804–809. doi:10.1038/nmat4687.

[2] D. Sciti, L. Zoli, L. Silvestroni, A. Cecere, G.D. Di Martino, R. Savino, Design, fabrication and high velocity oxy-fuel torch tests of a C_f-ZrB_2 - fiber nozzle to evaluate its potential in rocket motors, Mater. Des. 109 (2016) 709–717. doi:10.1016/j.matdes.2016.07.090.

[3] X. Jin, X. Fan, C. Lu, T. Wang, Advances in oxidation and ablation resistance of high and ultra-high temperature ceramics modified or coated carbon/carbon composites, J. Eur. Ceram. Soc. 38 (2017) 1–28. doi:10.1016/j.jeurceramsoc.2017.08.013.

[4] A. Riccio, F. Raimondo, A. Sellitto, V. Carandente, R. Scigliano, D. Tescione, Optimum design of ablative thermal protection systems for atmospheric entry vehicles, Appl. Therm. Eng. 119 (2017) 541–552. doi:10.1016/j.applthermaleng.2017.03.053.

[5] S.R. Levine, E.J. Opila, M.C. Halbig, J.D. Kiser, M. Singh, J.A. Salem, Evaluation of ultra-high temperature ceramics for aeropropulsion use, J. Eur. Ceram. Soc. 22 (2002) 2757–2767. doi:10.1016/S0955-2219(02)00140-1.

[6] S. Tang, J. Deng, S. Wang, W. Liu, K. Yang, Ablation behaviors of ultra-high temperature ceramic composites, Mater. Sci. Eng. A. 465 (2007) 1–7. doi:10.1016/j.msea.2007.02.040.

[7] A. Paul, V. Rubio, J. Binner, B. Vaidhyanathan, A. Heaton, P. Brown, Evaluation of the high

temperature performance of HfB_2 UHTC particulate filled C_f/C composites, Int. J. Appl. Ceram. Technol. 14 (2017) 344–353. doi:10.1111/ijac.12659.

[8] Z. Wang, S. Dong, X. Zhang, H. Zhou, D. Wu, Q. Zhou, D. Jiang, Fabrication and properties of C_f/SiC-ZrC composites, Journal of the American Ceramic Society. 91 (2008) 3434–3436. doi:10.1111/j.1551-2916.2008.02632.x.

[9] N. Padmavathi, S. Kumari, B.V.V. Prasad, J. Subrahmanyam, K.K. Ray, Processing of carbon-fiber reinforced (SiC + ZrC) mini-composites by soft-solution approach and their characterization, Ceram. Int. 35 (2009) 3447–3454. doi:10.1016/j.ceramint.2009.06.016.

[10] H. Hu, Q. Wang, Z. Chen, C. Zhang, Y. Zhang, J. Wang, Preparation and characterization of C/SiC–ZrB_2 composites by precursor infiltration and pyrolysis process, Ceram. Int. 36 (2010) 1011–1016. doi:10.1016/j.ceramint.2009.11.015.

[11] H. Pi, S. Fan, Y. Wang, C/SiC–ZrB_2–ZrC composites fabricated by reactive melt infiltration with $ZrSi_2$ alloy, Ceram. Int. 38 (2012) 6541–6548. doi:10.1016/j.ceramint.2012.05.035.

[12] S. Chen, C. Zhang, Y. Zhang, H. Hu, Preparation and properties of carbon fiber reinforced ZrC–ZrB_2 based composites via reactive melt infiltration, Composites Part B. 60 (2014) 222–226. doi:10.1016/j.compositesb.2013.12.067.

[13] A. Sayir, Carbon fiber reinforced hafnium carbide composite, J. Mater. Sci. 39 (2004) 5995–6003.

[14] L. Zou, N. Wali, J.-M. Yang, N.P. Bansal, Microstructural development of a C_f/ZrC composite manufactured by reactive melt infiltration, J. Eur. Ceram. Soc. 30 (2010) 1527–1535. doi:10.1016/j.jeurceramsoc.2009.10.016.

[15] D. Zhao, C. Zhang, H. Hu, Y. Zhang, Preparation and characterization of three-dimensional carbon fiber reinforced zirconium carbide composite by precursor infiltration and pyrolysis process, Ceram. Int. 37 (2011) 2089–2093. doi:10.1016/j.ceramint.2011.02.024.

[16] J. Lamon, Interfaces and Interphases, in: W. Krenkel (Ed.), Ceramic Matrix Composites, Wiley-VCH Verlag GmbH & Co. KGaA, Weinheim, Germany, 2008: pp. 49–68. doi:10.1002/9783527622412.ch3.

[17] W.G. Fahrenholtz, E.J. Wuchina, W.E. Lee, Y. Zhou, Introduction, in: W.G. Fahrenholtz, E.J. Wuchina, W.E. Lee, Y. Zhou (Eds.), Ultra-High Temperature Ceramics, John Wiley & Sons, Inc,

Hoboken, NJ, 2014: pp. 1–5. doi:10.1002/9781118700853.ch1.

[18] E.W. Neuman, G.E. Hilmas, W.G. Fahrenholtz, Mechanical behavior of zirconium diboride–silicon carbide–boron carbide ceramics up to 2200°C, J. Eur. Ceram. Soc. 35 (2015) 463–476. doi:10.1016/j.jeurceramsoc.2014.09.021.

[19] A. Vinci, L. Zoli, E. Landi, D. Sciti, Oxidation behaviour of a continuous carbon fibre reinforced ZrB_2 –SiC composite, Corros. Sci. 123 (2017) 129–138. doi:10.1016/j.corsci.2017.04.012.

[20] F. Monteverde, S. Guicciardi, A. Bellosi, Advances in microstructure and mechanical properties of zirconium diboride based ceramics, Mater. Sci. Eng. A. 346 (2003) 310–319. doi:10.1016/S0921-5093(02)00520-8.

[21] L. Zoli, D. Sciti, Efficacy of a ZrB_2–SiC matrix in protecting C fibres from oxidation in novel UHTCMC materials, Mater. Des. 113 (2017) 207–213. doi:10.1016/j.matdes.2016.09.104.

[22] D. Sciti, A.N. Murri, V. Medri, L. Zoli, Continuous C fibre composites with a porous ZrB_2 matrix, Mater. Des. 85 (2015) 127–134. doi:10.1016/j.matdes.2015.06.136.

[23] L. Zoli, A. Vinci, L. Silvestroni, D. Sciti, M. Reece, S. Grasso, Rapid spark plasma sintering to produce dense UHTCs reinforced with undamaged carbon fibres, Mater. Des. 130 (2017) 1–7. doi:10.1016/j.matdes.2017.05.029.

[24] A. Vinci, L. Zoli, D. Sciti, C. Melandri, S. Guicciardi, Understanding the mechanical properties of novel UHTCMCs through random forest and regression tree analysis, Mater. Des. 145 (2018) 97–107. doi:10.1016/j.matdes.2018.02.061.

[25] L. Zoli, A. Vinci, P. Galizia, C. Melandri, D. Sciti, On the thermal shock resistance and mechanical properties of novel unidirectional UHTCMCs for extreme environments, Sci. Rep. 8 (2018) 9148. doi:10.1038/s41598-018-27328-x.

[26] P. Galizia, S. Failla, L. Zoli, D. Sciti, Tough salami-inspired C_f/ZrB_2 UHTCMCs produced by electrophoretic deposition, J. Eur. Ceram. Soc. 38 (2018) 403–409. doi:10.1016/j.jeurceramsoc.2017.09.047.

[27] R. Savino, L. Criscuolo, G.D. Di Martino, S. Mungiguerra, Aero-thermo-chemical characterization of ultra-high-temperature ceramics for aerospace applications, J. Eur. Ceram. Soc. 38 (2018) 2937-2953. doi: 10.1016/j.jeurceramsoc.2017.12.043

[28] F. Monteverde, A. Cecere, R. Savino, Thermo-chemical surface instabilities of SiC-ZrB_2 ceramics in high enthalpy dissociated supersonic airflows, J. Eur. Ceram. Soc. 37 (2017) 2325-2341. doi:10.1016/j.jeurceramsoc.2017.01.018

[29] C. Pradere, C. Sauder, Transverse and longitudinal coefficient of thermal expansion of carbon fibers at high temperatures (300–2500 K), Carbon. 46 (2008) 1874–1884. doi:10.1016/j.carbon.2008.07.035.

[30] D. Aveston, A. Kelly, Theory of multiple fracture of fibrous composites, J. Mater. Sci. 8 (1973) 352–362. doi:10.1007/BF00550155.

[31] Y. Shi, N. Jain, D. Koch, Investigation and modeling of tensile failure properties of wound ceramic matrix composites, Composites Part A. 114 (2018) 316–326. doi:10.1016/j.compositesa.2018.08.029.

[32] U. Santhosh, J. Ahmad, S. Kalarikkal, G. Ojard, Y. Gowayed, Time-dependent deformation and damage modeling of a SiC/SiC composite, J Aerospace Eng. 31 (2018) 04018086. doi:10.1061/(ASCE)AS.1943-5525.0000921.

[33] R. Kulkarni, O. Ochoa, Transverse and longitudinal CTE measurements of carbon fibers and their impact on interfacial residual stresses in composites, J. Compos. Mater. 40 (2006) 733–754. doi:10.1177/0021998305055545.

[34] R.A. Schapery, Thermal expansion coefficients of composite materials based on energy principles, J. Compos. Mater. 2 (1968) 380–404. doi:10.1177/002199836800200308.

[35] R.W. Rice, Evaluation and extension of physical property-porosity models based on minimum solid area, J. Mater. Sci. 31 (1996) 102–118. doi:10.1007/BF00355133.

[36] F. Monteverde, A. Bellosi, Effect of the addition of silicon nitride on sintering behaviour and microstructure of zirconium diboride, Scr. Mater. 46 (2002) 223–228. doi:10.1016/S1359-6462(01)01229-5.

[37] J.B. Wachtman, W.E. Tefft, D.G. Lam, C.S. Apstein, Exponential temperature dependence of Young's modulus forseveral oxides, Phys. Rev. 122 (1961) 1754–1759. doi:10.1103/PhysRev.122.1754.

[38] S. Guicciardi, A.K. Swarnakar, O. Van Der Biest, D. Sciti, Temperature dependence of the dynamic Young's modulus of ZrB_2–$MoSi_2$ ultra-refractory ceramic composites, Scr. Mater. 62 (2010) 831–

834. doi:10.1016/j.scriptamat.2010.02.011.

[39] P. Boch, J.-C. Niepce, Ceramic materials: processes, properties and applications, ISTE, London, 2007. doi:10.1002/9780470612415.

[40] D.J. Green, An introduction to the mechanical properties of ceramics, Cambridge University Press, 1998. doi:10.1017/CBO9780511623103.

[41] A.G. Evans, F.W. Zok, R.M. McMeeking, Fatigue of ceramic matrix composites, Acta Mater. 43 (1995) 859–875. doi:10.1016/0956-7151(94)00304-Z.

[42] G. Fang, X. Gao, G. Yu, S. Zhang, J. Chen, Y. Song, Effect of the stress level on the fatigue strengthening behavior of 2D needled C/SiC CMCs at room temperature, Mater. Des. 89 (2016) 432–438. doi:10.1016/J.MATDES.2015.10.013.

[43] U. Ramamurty, J.C. McNulty, M. Stenn, Fatigue in Ceramic Matrix Composites, in: A. Kelly, C. Zweben (Eds.), Comprehensive composite materials, Elsevier, 2000: pp. 163–219. doi:10.1016/B0-08-042993-9/00093-0.

[44] F.D. Gac, Is there anything of practical value hidden amongst the composite-toughening theories?!-A Jim Mueller perspective, in: J.B. Wachtman Jr (Ed.), A collection of papers presented at the 14th annual conference on composites and advanced ceramic materials: ceramic engineering and science proceedings, The American Ceramic Society, Inc., Westervill, 1990: pp. 551–570. doi:10.1002/9780470313008.ch1.

[45] G. Ziegler, Importance of interface, in: G. De Portu (Ed.), Introduction to mechanical behaviour of ceramics, Consiglio nazionale delle ricerche, Faenza, 1992: pp. 208–213.

[46] P. Reynaud, D. Rouby, G. Fantozzi, Effects of temperature and of oxidation on the interfacial shear stress between fibres and matrix in ceramic-matrix composites, Acta Mater. 46 (1998) 2461–2469. doi:10.1016/S1359-6454(98)80029-3.

[47] M.X. Shi, B. Liu, Z.Q. Zhang, Y.W. Zhang, H.J. Gao, Direct influence of residual stress on the bending stiffness of cantilever beams, Proc. R. Soc. A. 468 (2012) 2595–2613. doi:10.1098/rspa.2011.0662.

[48] L. Yang, Y. Yan, J. Ma, B. Liu, Effects of inter-fiber spacing and thermal residual stress on transverse failure of fiber-reinforced polymer-matrix composites, Comput. Mater. Sci. 68 (2013)

255–262. doi:10.1016/j.commatsci.2012.09.027.

[49] J.G. Goree, R.S. Gross, Analysis of a unidirectional composite containing broken fibers and matrix damage, Eng. Fract. Mech. 13 (1980) 563–578. doi:10.1016/0013-7944(80)90086-7.

[50] S. Ochiai, H. Tanaka, S. Kimura, M. Tanaka, M. Hojo, K. Okuda, Modeling of residual stress-induced stress–strain behavior of unidirectional brittle fiber/brittle matrix composite with weak interface, Compos. Sci. Technol. 63 (2003) 1027–1040. doi:10.1016/S0266-3538(03)00015-0.

Figure Captions

Fig.1. SEM micrographs of polished cross section of *UHTCMC* based on pitch-derived carbon fibers and ZrB_2/SiC matrix along (a) the transverse direction, and (b) longitudinal direction. (c) Fracture surface along the longitudinal direction (the arrows point the presence of cracks in the matrix). *(two- column)*

Fig.2. (a) Relative dimensional change ($\Delta L/L_0$) vs. temperature of the tested *UD* samples (blue line with square symbols), and pitch-derived fibers C_f [29] (red line with circle symbols) along the transverse (*t* subscript, half up symbols) and the longitudinal (*l* subscript, half right symbols) direction, and polycrystalline ZrB_2 [20] (gray line with open triangle symbol). (b) Anisotropy degree *R* vs. temperature of tested *UD* (blue line with marked square symbol), C_f (red line with marked circle symbol), and theoretical *UD* trend (green line with solid star symbol). *(two- column)*

Fig.3. Relative dimensional change ($\Delta L/L_0$) along *l*-direction vs. temperature of the tested *UD* samples (blue line with square symbols), theoretical trend (green line with half right star symbols), and adjusted trend which take into account the matrix damaging/softening (black line with open star symbols). *(single column)*

Fig.4. Theoretical residual stresses into matrix (gray line with open triangle symbol) and fibers (red line with half right circle symbols) that should develop during cooling. *(single column)*

Fig.5. (a) Relative dimensional change ($\Delta L/L_0$) along *l*-direction during three consecutive thermal cycles (labeled with roman numbers) between *RT* and 1300 °C. Each thermal step is numbered in chronological order. (b) Relative dimensional change ($\Delta L/L_0$) along *l*-direction for each heating step together with the $\Delta L/L_0$ of typical anisotropic pitch-derived carbon fibers (C_f) [27], and that of *UD* samples after sintering (plotted also in Fig.2). The curves were scaled by updating the L_0 value after each thermal cycle. *(two- column)*

Fig.6. Scheme of the stress – strain variation after applying a compressive (a) and tensile (b) external load into a continuous fiber-reinforced composite with initial/residual thermal stresses. The arrows flow from the

initial point (open symbols) to the final point (solid symbols) for both fiber (circle symbols) and matrix (square symbols). The areas filled with lines pattern (horizontal for matrix, vertical for fiber) correspond to the initial/bounded energy density. The solid areas correspond to deformation work done by the external applied force. *(two- column)*

Graphical Abstract

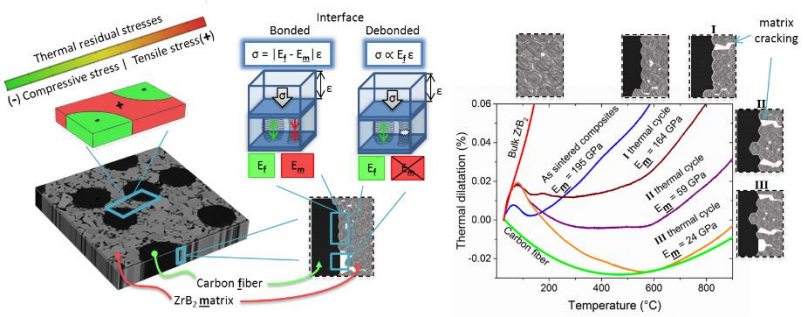

Highlights

- Thermal cycles induce matrix cracking which decreases the Young's modulus of the ZrB_2-based matrix from 195 GPa to 24 GPa.
- The longitudinal thermal dilatation of the composites decreases by thermal cycling and approaches the dilatation behavior of bare carbon fibers.
- Contrary to linear elasticity the composite Young's modulus is affected by residual stresses even in absence of micro-damage.
- A new equation replacing Voigt's model is proposed to account for residual stresses effect and damage frequency on Young's modulus.